Journal of Environmental Chemical Engineering 10 (2022) 107577

Contents lists available at ScienceDirect

Journal of Environmental Chemical Engineering

journal homepage: www.elsevier.com/locate/jece

Investigation of the influence of the void fraction on the energy consumption of a vertical electrolyser under natural convection

Gabriel Wosiak [a], Jeyse da Silva [a], Sthefany S. Sena [a], Evaldo B. Carneiro-Neto [a], Mauro C. Lopes [b], Ernesto Pereira [a,*]

[a] Chemistry Department, Federal University of São Carlos, 13565-905, São Carlos, SP, Brazil
[b] Departamento de Química, Universidade Estadual do Centro-Oeste, 85040-080, Guarapuava, PR, Brazil

ARTICLE INFO

Editor: Despo Kassinos

Keywords:
Hydrogen generation
Electrolysis
Finite element simulation
Computational Fluid Dynamics
Electro-generated bubbles

ABSTRACT

The ongoing need to develop and enhance current energy sources to replace fossil fuels emphasizes the necessity of a thorough understanding of clean energy production methods such as hydrogen production via water electrolysis. This work provides a versatile CFD (Computational Fluid Dynamics) simulation that describes an alkaline water electrolyzer, which considers the electrolyte's performance, electrode materials, separator membrane, and the impact of generated bubbles in the electrolysis considering anodic and cathodic reactions at the same time. The bubble presence affects the applied cell potential and the local current distribution, and it is directly related to the efficiency of the process. For a multivariate view, a 2^3 factorial design was carried out, in which electrode material, applied current density, and the presence or absence of gas bubbles were simultaneously investigated. As a result, the contribution of each factor to the cell potential was calculated, their link to the applied current, and the cross-effects. Finally, we observed an important non-uniformity in the local current distribution and an increase in the spent energy due to the produced gases at current densities higher than 100 mA cm^{-2}.

1. Introduction

Since fossil fuels will run out, and, besides that, less harmful alternatives must be investigated, an inevitable shift in the global energy grid is beginning [1–3]. Hydrogen is one of the possible choices to replace the most used energy vector. However, nowadays, hydrogen production routes imply high energy consumption, making its commercial adoption on a large scale unfeasible [4,5]. The development of materials with improved electrocatalytic activity to create H_2, investigate the electrolyte composition to reduce ohmic drop, as well as membranes that allow ions to move between compartments while preventing the mixing of H_2 and O_2 gases created in each chamber, has been the key to getting around this stumbling block [6–10].

A few published papers have already shown that understanding the hydrodynamic properties and the electric field in an electrolyzer is essential to improving the device's efficiency [11–16]. The most low-cost and fast way to do this task is to perform computer simulations of the system. It is possible to evaluate several system variables using this methodology, such as flux, applied current density, solution conductivity, and even membrane and electrode materials, without modifying experimental conditions [17–19]. Then, the finite element technique is a potent tool for describing and solving differential equations under boundary conditions that do not have an analytic solution, both on an industrial and laboratory scale [20–22].

It is well understood that the system's thermodynamic potential is augmented by an extra amount of energy to drive the charge transfer reaction during an electrochemical process, known as overpotential. Nucleation, concentration, activation, polarization, and bubble resistance are examples of overpotentials [23–25]. For electrolyzers, all overpotentials mentioned deserve to be considered in an investigation to improve the whole system's efficiency. Important experimental and theoretical findings in the water splitting process have been reported previously by our and other research groups. The abrupt change in the pH close to the electrode surface leads to a major increase in the cell Overpotential [26,27]. The role of bubbles in convective transport and in blocking the electrode surface is another relevant point [28–30].

Considering what has been said, it is important to study the effect of bubbles and their interpretation with other aspects of electrolyser

* Corresponding author.
E-mail address: ernesto@ufscar.br (E. Pereira).

https://doi.org/10.1016/j.jece.2022.107577
Received 29 December 2021; Received in revised form 11 March 2022; Accepted 16 March 2022
Available online 24 March 2022

operation, so we need a complete model that solves the natural convection of the electrolyte along with the current and potential distribution and surface effects of the electrode.

As far as we know, there are just a few simulation studies dedicated to exploring a working mode for electrolyzers to identify paths with the potential to reduce energy consumption. Since many of these studies have focused on electrolyzers in forced convection environments, the present study will evaluate the role of natural convection on gas removal. This paper provides a model based on a geometry comparable to a commercial alkaline electrolyzer in this setting. The effects of activation overpotentials, polarization, and bubble resistance are all considered. In this model, the concentration overpotential was disregarded.

The Bruggeman correction was used to assess the contribution of bubble formation in the lowering of the electrolyte's effective conductivity [31]. We also took into account a drop in electrode activity (j_0) due to the surface bubble covering. When active sites are covered, the reaction cannot take place.

Furthermore, a 2^3 factorial design was used to investigate the effects of the variables: current density, electrode material, and the presence or absence of bubbles in the process. This study was able to provide a thorough understanding of the process by demonstrating which variables are most significant in cell potential fluctuation, as well as the cross-effects across the variables being researched.

2. Model

The model's geometry was created using a rectangular electrolysis cell as a reference, as stated by CFD Modeling of Electrolyzers [32–35]. The model was built based on a 2D Cartesian geometry, which considers two chambers separated by a membrane with thickness and conductivity specifications according to commercial membranes [36], as shown in Fig. 1. Both chambers contain the same electrolyte, the liquid water material present in the COMSOL Materials Library was modified according to dynamic viscosity, density and electric conductivity of KOH 6 mol L^{-1} [37,38]. The imposed potential difference takes the evolution of

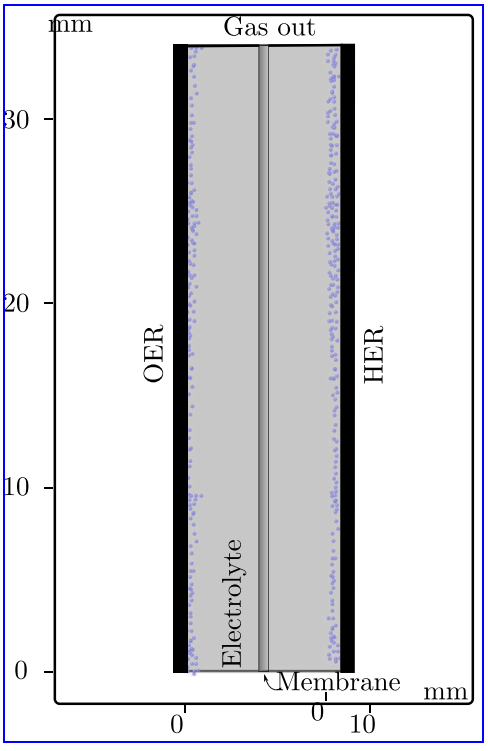

Fig. 1. Model used in the electrolyzer simulation.

oxygen over the anode in the left chamber and hydrogen over the cathode in the other. Each compartment is 15 mm wide. The set measures 100 mm in height and the electrodes occupy the entire outer sidewall of each chamber.

To describe the natural convection, the Euler-Euler model was used [31], which is based on the Navier-Stokes equations for a fluid that consists of a mixture of liquid and gas phases. This model considers that the relative movement between the liquid and gas phases is due to the balance of drag and pressure forces. Therefore, the mixture needs a momentum equation and three continuity equations, one related to the mixture and the other two for each phase.

$$\rho\frac{\partial u}{\partial t}+\rho(u\cdot\nabla)u = \nabla\cdot[-p\mathbf{I}+\mathbf{K}]+\rho\mathbf{g} \tag{1}$$

$$\frac{\partial\rho}{\partial t}+\nabla\cdot(\rho u)=0 \tag{2}$$

$$\frac{\partial\rho_j\epsilon_j}{\partial t}+\nabla\cdot\left(\rho_j\epsilon_j u_j\right)=0 \tag{3}$$

where, ρ is the density, u is the velocity vector, p is the pressure, g is the gravity vector, ϵ_j is the volume fraction of phase j, the $\mathbf{K}$ is the viscous stress tensor which incorporates all the terms related to turbulent fluid movement. In addition to these equations, the model also has two additional transport equations, one for turbulent kinetic energy and the other for turbulent dissipation rate, both of which serve to describe the spatiotemporal evolution of properties that can result in turbulent motions in the fluid.

As boundary condition, the model proposes that at the gas output interface, the fluid is subject only to the force of atmospheric pressure and the gas density is equal to that of air.

At each electrode/electrolyte interface, a flux boundary condition is obtained by simple mass balance disregarding any parallel reaction.

- To cathode

$$-\mathbf{n}\cdot\mathbf{N}=-\frac{j_{F,cathode}(y)M_{O_2}}{Fn_{O_2}} \tag{4}$$

- To anode

$$-\mathbf{n}\cdot\mathbf{N}=-\frac{j_{F,anode}(y)M_{H_2}}{Fn_{H_2}} \tag{5}$$

where, $\mathbf{n}\cdot\mathbf{N}$ is the normal flux of gas formation at the electrode/electrolyte interfaces, $j_{F,cathode}$ and $j_{F,anode}$ are the faradaic current densities at the cathode and the anode, respectively, which are functions of the position on the electrode surface, y. M_{O_2} and M_{H_2} are, in this order, the molar masses of the oxygen and hydrogen gases, while n_{O_2} and n_{H_2} are the number of transferred electrons in oxygen and hydrogen evolution reactions, respectively [27].

A secondary current distribution was used to model the potential distribution inside the system.

$$\nabla\cdot(-\sigma\nabla\phi)=0 \tag{6}$$

where, σ is the electrolyte or membrane conductivity and ϕ is the electrolyte or membrane potential.

Here, the Bruggeman correction[25] takes its place since the effective conductivity of the electrolyte in each area element is calculated regarding the local fraction of gas present at each instant:

$$\sigma_{eff}=\sigma\left(1-\epsilon_g\right)^{\frac{3}{2}} \tag{7}$$

where, ϵ_g is the gas volume fraction.

The equation 6 is subject to the following boundary conditions:

$$j_{app}\ l_{cathode} + \int_{cathode} \left[-j_{F,cathode}\left(\phi_{DL,cathode}\right) \right] - j_{C,cathode}\left(\phi_{DL,cathode}\right) \Big] dy = 0, \tag{8}$$

where $l_{cathode} = \int_{cathode} dy$

$$\phi_{ext,anode}(t) = 0 \tag{9}$$

$$\phi_{ext,cathode}(t) = \phi_{DL,cathode}(y,t) + \phi_{OHP,cathode}(y,t) = \phi_{DL,anode}(y,t) + \phi_{OHP,anode}(y,t) \tag{10}$$

where, j_{app} is the applied current density, $j_{F,cathode}$ and $j_{C,cathode}$ are the local faradaic and capacitive current densities at the cathode, respectively, which are functions of electric double layer potential at the cathode, $\phi_{DL,cathode}$. $\phi_{DL,anode}$ is the electric double layer potential at the anode, while $\phi_{ext,cathode}$ and $\phi_{OHP,cathode}$ are, in order, the external potential at the cathode and the electrolyte potential at the outer Helmholtz plane of this electrode, whereas $\phi_{ext,anode}$ and $\phi_{OHP,anode}$ are the same variables for the anode.

The boundary condition 8, through integration on the cathode surface, expresses that all current applied to the electrode must be divided into two contributions, one capacitive and the other faradaic. A variation in the electric double layer potential is used to ensure this relationship, resulting in a convenient change in the external potential. Due to the relativity of the potential scale, a reference for the system must be defined to obtain a unique solution to ensure simulation convergence. Equation 9 describes it by imposing that the external potential of the anode is zero. Thus, Kirchhoff's second law applied to the system yields equation 10 that relates the potential contributions spent in each of the processes that make up the electrolyzer.

As already mentioned, the total current breaks down into its capacitive and faradaic components. Thus, the following expressions describe the capacitive currents.

$$j_{C,cathode} = C_{DL,cathode}\frac{\partial \phi_{DL,cathode}}{\partial t} \tag{11}$$

$$j_{C,anode} = C_{DL,anode}\frac{\partial \phi_{DL,anode}}{\partial t} \tag{12}$$

where, $C_{DL,cathode}$ and $C_{DL,anode}$ are the specific capacitances of the cathode and anode, respectively.

Faradaic currents correspond to the charge transfer processes between electrodes and electrolytes at the interfaces. Therefore, the Tafel model for both electrodes was assumed to describe them, as listed below.

$$j_{F,cathode}(y) = -j_{0,H_2,eff}\ 10^{\frac{\left(\phi_{DL,cathode} - E^{0\prime}_{H_2}\right)}{A_C}} \tag{13}$$

$$j_{F,anode}(y) = j_{0,O_2,eff}\ 10^{\left(\phi_{DL,anode} - E^{0\prime}{}_{O_2}\right)/\mathrm{A_A}} \tag{14}$$

where, A_C and A_A are the Tafel slopes, $j_{0,H_2,eff}$ and $j_{0,O_2,eff}$ are the effective exchange current densities which incorporate the free area fraction, that is, not covered by gas. For this purpose, the correction takes into account the gas fraction that covers the surface of the electrodes, assuming that the bubbles on the surface are perfectly hemispherical, identical in size, and are all bonded with a 90° contact angle. Based on these assumptions, it is obtained that this correction is performed by multiplying the exchange current density with the factor $1 - \frac{3}{2}\epsilon_g$ (for more details, refers to Section 1 of the SI). The kinetics parameters are showed in Table 1.

The set of equations was solved by numerical simulation using the finite element method, implemented in the software COMSOL Multiphysics in version 5.6 running in the GNU/Linux Ubuntu 18.04 LTS. The calculations were performed on a computer with an i7 processor and 128 GB of RAM. The chosen mesh contains around 350,174 elements, and some variations may occur due to local refinements that depend on the size chosen for the gas bubbles. The computational time depends on the coupled physics, and the main parameter is the applied current density. For instance, at 300 mA cm^{-2}, the computational time was about 2 h.

Table 1
Exchange current densities and Tafel slopes for hydrogen evolution reaction and oxygen evolution reaction on nickel and platinum[39].

	Ni	Pt
j_{0,H_2} /A m^{-2}	1.1 10^{-2}	4.0
j_{0,O_2} /A m^{-2}	4.2 10^{-2}	1.2 10^{-5}
A_C /mV	121	105
A_A /mV	95	46

3. Results and discussion

3.1. Current distribution

One of the advantages of the simulations is that it is possible to verify the localized behavior of the physical quantities that, experimentally, are only accessible as an average value. Thereby, the Fig. 2(A) shows the effective electrolyte conductivity 7, that depends on the gas fraction on the domain. The produced H_2 volume is approximately twice that of O_2 due to the reaction stoichiometry. For this reason, the effective conductivity is lower at the catholyte, it result in a distortion in the equipotential lines, and, consequently, in the current paths (white lines). In addition, the buoyancy force induces the bubbles to accumulate at the top of the domain (see the video in the supporting material). Consequently, there is a reduction in the conductivity where bubbles aggregate.

Concerning the electrical potential, both in the electrolyte and inside the membrane, there is a considerable change in the colors when comparing anode and cathode chambers, which indicates that flowing current through the membrane demands significant potential. The membrane conductivity is usually much lower than the electrolyte conductivity, as expected. As can be seen in Fig. 2(B), the current paths (white lines) indicate a non-uniformity in the current density along the electrode surface, with a higher density of lines at the bottom of the domain. Which means that in this region there is a greater preference for the passage of current due to the lower impediment effect related to the presence of void fractions.

Fig. 3 A and 3B show that the end of the upper edge contributes with less current due to the partial blockage by bubbles, in which it is observed that the coating by bubbles tends to be more significant in the upper part of the electrode. Thus a smaller fraction from the electrode area has access to the electrolyte and thus can contribute to the charge transfer reaction. This coating also varies depending on the applied current density. The greater the applied current density, the more vigorous the bubble formation and, therefore, higher coverage is observed. In addition, due to the buoyant force the bubbles are subject to, they tend to move within the liquid phase against gravity. A mode detailed visualization is provided in the video in the Supporting Material, which shows the electrolysis along the time. Part of the produced bubbles tends to spread in the chamber, following their self convection, and consequently, there is a gas accumulation that have impact in the electrolyte conductivity and electrode performance. However, in the detachment process, the bubbles eventually collide with other bubbles and coalesce and may or may not adhere to the surface. For this reason, the approach used in the simulations estimates the coating fraction as a function of the gas volume fraction close to the electrode surfaces, disregarding any interaction force between the bubble and the electrode surface since the model does not track bubbles individually.

Of course, the variable that carries with it all the contributions of the different overpotentials is the cell potential. Furthermore, it is directly related to energy consumption since it was established in the simulation

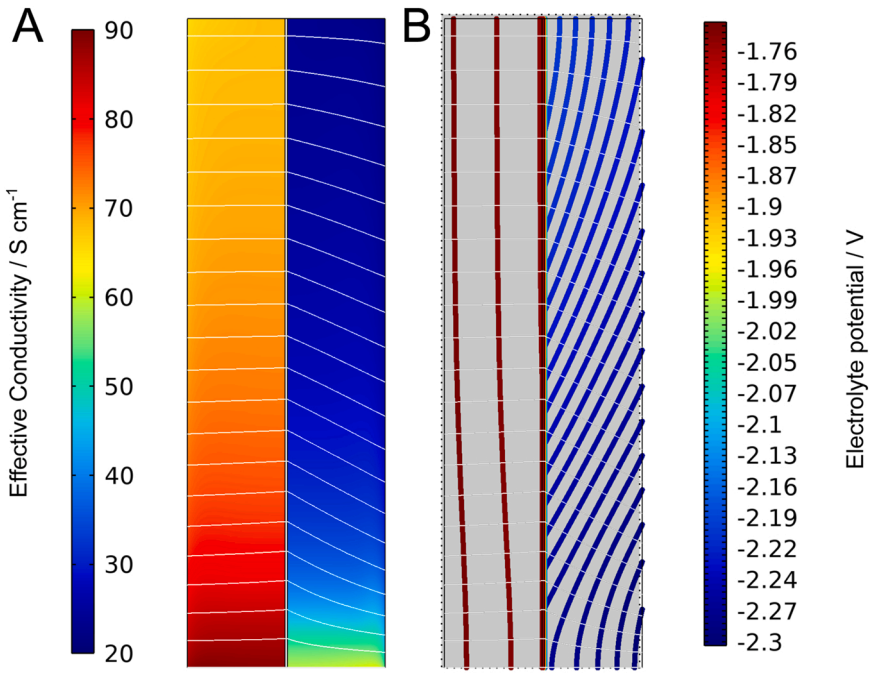

Fig. 2. (A) Surface plot of the electrolyte conductivity considering the Bruggeman correction. (B) Electrolyte potential represented by colored equipotential lines. White lines represent the current paths. t = 22.5 s, j = 630 mA cm^{-2}.

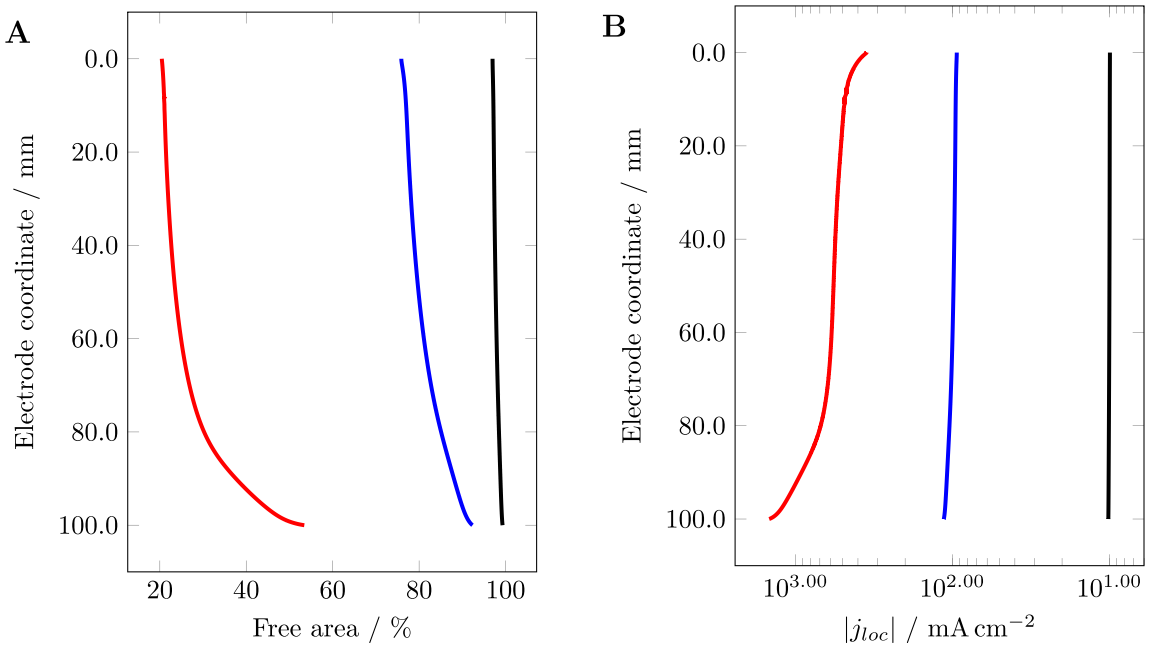

Fig. 3. (A) Free area and (B) local current at cathode surface in different values of applied current density. 10 (black), 100 (blue) and 630 (red) mA cm^{-2}.

that the electrolyzer operates in galvanostatic mode. So then, the comparison between potentials of cells with different assumptions can allow us to assign contributions relative to each overpotential.

Fig. 4 shows the comparison between the cases in which the corrections for the specific conductivity of the electrolyte and the current exchange density, due to the presence of bubbles, were disregarded (filled circles) and considered (open circles). The difference between the curves becomes remarkable only at current densities greater than 100 mA cm^{-2}, when the presence of bubbles begins to represent an increasing portion of cell potential required to keep the applied current constant. In other words, the existence of bubbles means a significant contribution to the total energy consumption of the electrolyzer.

Comparing the curves with and without bubbles allows us to estimate the bubble overpotential and thus evaluate its relative contribution to the cell potential. For example, when Pt is used as the cathode and Ni as the anode, the bubble overpotential is about 65 mV for j_{app} = 398.1 mA cm^{-2} and 154 mV when j_{app} = 631.0 mA cm^{-2}, indicating that, by this model, the contribution of bubbles in the cell potential increases with increasing applied current density. In the first case, approximately 2.7% of the energy consumed in the electrolyzer operation is spent on compensating for the void fraction effects. In contrast, this contribution represents about 5.7% of the total energy expended for

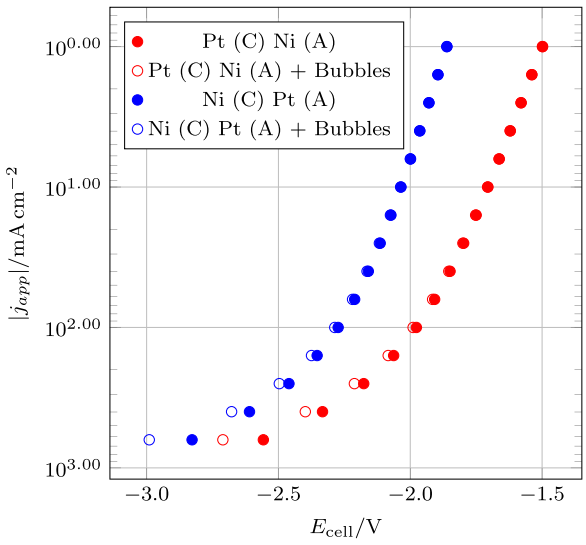

Fig. 4. Comparison of Polarization curve between two electrode configurations.

the second case. Similar values were obtained when the electrodes were considered in an inverted configuration: Pt as anode and Ni as the cathode.

3.2. Chemometric study

A factorial design was carried out to map the effects of three selected variables on the behavior of cell potential, using two distinct levels. The evaluated variables were: .

- The current density;
- Electrode material alternating between Pt and Ni;
- Neglecting or considering corrections related to void fractions.

The combinations between these variables resulted in 8 sets of data presented in Table 2.

The Daniel plot, shown in Fig. 5A, is an plot that identifies estimated effects in an experiment that are large relative to the noise. The closer the effect is to the vertical red line, the less statistically significant is this effect. And the effects further away from the zero line are more significant. Fig. 5B shows the influence of the variables and cross-effects between them in the applied cell potential. Because this data set is not repeatable for being a simulation, the median of the small impacts (near to the Daniel plot line) was utilized to compute a pseudo standard error using the Lenth technique [40]. Then, two approaches were employed to determine the marginal error (ME) and the simultaneous marginal error (SME). The SME differs from the ME in that it is a somewhat more discriminating metric. This lines (ME and SME) are what define if an effect is significant, or not. The Pareto plot (Fig. 5B), also shows that the choice of the electrodes configuration and the applied current density are the main parameters. The arrangement employing Pt electrode for

Table 2
Parameters and response of the 2^3 Design of Experiments. Data from Fig. 4.

Exp	Bubbles	Electrodes	j_{app} (mA cm^{-2})	E_{cell} (V)
1	No	Pt(C) Ni (A)	-398	-2.333
2	Yes	Pt(C) Ni (A)	-398	-2.398
3	No	Ni (C) Pt (A)	-398	-2.610
4	Yes	Ni (C) Pt (A)	-398	-2.678
5	No	Pt(C) Ni (A)	-630	-2.557
6	Yes	Pt(C) Ni (A)	-630	-2.711
7	No	Ni (C) Pt (A)	-630	-2.828
8	Yes	Ni (C) Pt (A)	-630	-2.990

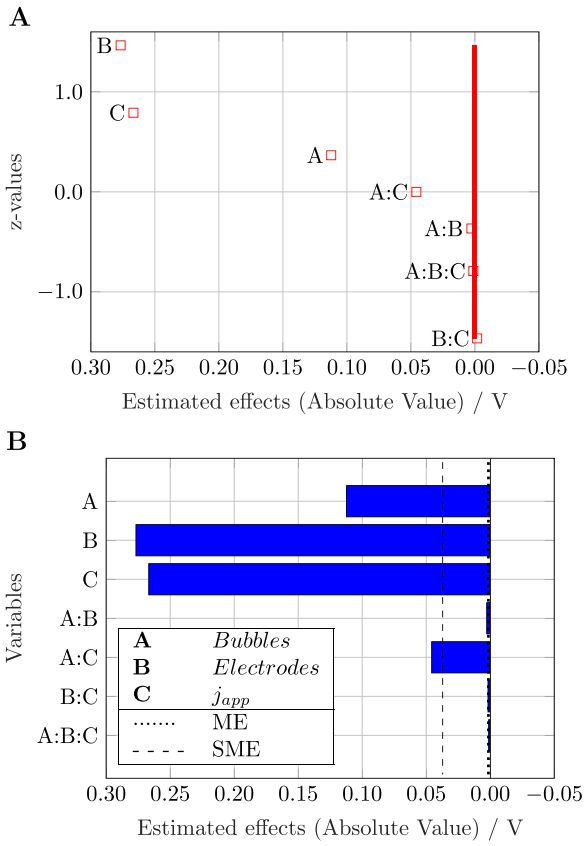

Fig. 5. Daniel Plot (probability) (A) and Pareto (B) plots of the choosen variables in applied cell potential, with the significance lines: marginal error (ME) and the simultaneous marginal error (SME).

HER and Ni electrode for OER requires the less negative applied potential for the same applied current density than the opposite configuration, which was an expected result due to the higher catalytic activity of Pt for the HER. There is no interaction between these two main variables. The third main variable is the presence of the bubbles, which has a negative effect. Since this chemometric study focuses on how bubbles affect the cell potential, it can be seen in Table 2 and Fig. 4 that E_{cell} it gets more negative due to the presence of bubbles through the range of studied current densities. However, the presence of bubbles has other implications. The first one is concerned with the accumulation of bubbles onto the electroactive area of the electrode, which leads to a reduction of available active sites to the reaction occur; The second way is with respect to the accumulation of bubbles throughout the chambers, which implies in an electrolyte conductivity decrease.

The only observed cross-effect is between electrode configuration and bubbles presence. It is due to the considered correction in the exchange current, which depends on the bubble fraction at the electrode surface. The configuration with Ni for HER and Pt for OER has a more prominent bubble overpotential because this configuration has a larger component of activation overpotential.

4. Conclusions

In this work, we provide a versatile simulation that can show the electrochemical and fluid-dynamic behavior of a water-splitting reactor, considering the electrodes kinetics, membrane, and, especially, the presence of gas bubbles in the whole domain. These variables affect the electrolyte conductivity, the available active sites, the spent energy to reaction occur, and induce a non-uniform current density at the surface of the electrodes, which can not be explained only by border effect. Thus, the larger the current density, the more significant the

contribution of bubbles in the process.

CRediT authorship contribution statement

Gabriel Wosiak: Conceptualization, Methodology, Software, Investigation, Data Curation, Writing – original draft, Visualization. **Jeyse da Silva:** Formal analysis, Investigation, Data curation, Writing – original draft, Visualization. **Sthefany S. Sena:** Investigation, Data curation, Writing – original draft, Visualization. **Evaldo B. Carneiro-Neto:** Conceptualization, Writing – original draft. **Mauro C. Lopes:** Writing – review & editing, Supervision. **Ernesto Pereira:** Resources, Writing – review & editing, Supervision, Project administration, Funding acquisition.

Declaration of Competing Interest

The authors declare that they have no known competing financial interests or personal relationships that could have appeared to influence the work reported in this paper.

Acknowledgments

The authors gratefully acknowledge support from FAPESP (São Paulo Research Foundation, Grant Numbers 2013/07296-2, 2014/50249-8, 2017/11986-5, 2018/24383-0, 2019/27029-5, 2021/03592-2), Shell and the strategic importance of the support given by ANP (Brazil's National Oil, Natural Gas and Biofuels Agency) through the R \&D levy regulation, CNPq, and CAPES (Code 001).

Appendix A. Supporting information

Supplementary data associated with this article can be found in the online version at doi:10.1016/j.jece.2022.107577.

References

[1] J. Andrews, B. Shabani, The role of hydrogen in a global sustainable energy strategy, WIREs Energy Environ. 3 (2014) 474–489, https://doi.org/10.1002/wene.103.

[2] B., van Ruijven, J.-F., Lamarque, D.P., van Vuuren, T., Kram, H., Eerens, Emission scenarios for a global hydrogen economy and the consequences for global air pollution, Global Environmental Change 21 (2011) 983–994.10.1016/j.gloenvcha.2011.03.013, symposium on Social Theory and the Environment in the New World (dis)Order.

[3] R. Derwent, P. Simmonds, S. O'Doherty, A. Manning, W. Collins, D. Stevenson, Global environmental impacts of the hydrogen economy, Int. J. Nucl. Hydrog. Prod. Appl. 1 (2006) 57–67, https://doi.org/10.1504/IJNHPA.2006.009869.

[4] S. Blanchette, A hydrogen economy and its impact on the world as we know it, Energy Policy 36 (2008) 522–530, https://doi.org/10.1016/j.enpol.2007.09.029.

[5] K., Urbaniec, A., Friedl, D., Huisingh, P., Claassen, Hydrogen for a sustainable global economy, Journal of Cleaner Production 18 (2010) S1-S3.10.1016/j.jclepro.2010.05.010, sustainable Hydrogen from Biomass.

[6] D.V. Esposito, Membraneless electrolyzers for low-cost hydrogen production in a renewable energy future, Joule 1 (2017) 651–658, https://doi.org/10.1016/j.joule.2017.07.003.

[7] F. Grüger, O. Hoch, J. Hartmann, M. Robinius, D. Stolten, Optimized electrolyzer operation: employing forecasts of wind energy availability, hydrogen demand, and electricity prices, Int. J. Hydrog. Energy (2019) 4387–4397, https://doi.org/10.1016/j.ijhydene.2018.07.165.

[8] D.M.F. Santos, C.A.C. Sequeira, J.L. Figueiredo, Hydrogen production by alkaline water electrolysis, Quím. Nova 36 (2013) 1176–1193, https://doi.org/10.1590/S0100-40422013000800017.

[9] S.M.H. Hashemi, M.A. Modestino, D. Psaltis, A membrane-less electrolyzer for hydrogen production across the pH scale, Energy Environ. Sci. 8 (2015) 2003–2009, https://doi.org/10.1039/C5EE00083A.

[10] A., Chalgin, C., Song, P., Tao, W., Shang, T., Deng, J., Wu, Effect of supporting materials on the electrocatalytic activity, stability and selectivity of noble metal-based catalysts for oxygen reduction and hydrogen evolution reactions, Progress in Natural Science: Materials International 30 (2020).10.1016/j.pnsc.2020.01.003.

[11] Y.-H. Li, Y.-J. Chen, The effect of magnetic field on the dynamics of gas bubbles in water electrolysis, Sci. Rep. 11 (2021) 9346, https://doi.org/10.1038/s41598-021-87947-9.

[12] C.-L. Liu, Z. Sun, G.-M. Lu, J.-G. Yu, Hydrodynamic characteristics of the two-phase flow field at gas-evolving electrodes: numerical and experimental studies, R. Soc. Open Sci. 5 (2018), 171255, https://doi.org/10.1098/rsos.171255. ⟨https://pubmed.ncbi.nlm.nih.gov/29892347https://www.ncbi.nlm.nih.gov/pmc/articles/PMC5990747/⟩.

[13] P. Mandin, H. Roustan, R. Wthrich, J. Hamburger, G. Picard, Two-phase electrolysis process modelling: from the bubble to the electrochemical cell scale, WIT Trans. Eng. Sci. 54 (2007) 73–87, https://doi.org/10.2495/ECOR070081.

[14] A. Filippov, I. Korotkin, I. Urazov, O. Ushakova, V. Vasil'ev, Thermo-electrical regime of a vertical electrolyzer: estimates of the effects of electric conductivity and gas evolution, J. Eng. Thermophys. 17 (2008) 218–226.

[15] W. El-Askary, I. Sakr, K. Ibrahim, A. Balabel, Hydrodynamics characteristics of hydrogen evolution process through electrolysis: numerical and experimental studies, Energy 90 (2015) 722–737.

[16] J., Rodríguez, E., Amores, Cfd modeling and experimental validation of an alkaline water electrolysis cell for hydrogen production, Processes 8 (2020).⟨https://www.mdpi.com/2227–9717/8/12/1634⟩.10.3390/pr8121634.

[17] J. Bisang, Theoretical and experimental studies of current distribution in gas-evolving electrochemical reactors with parallel-plate electrodes, J. Appl. Electrochem. 21 (1991) 760–766.

[18] L. Mustoe, A. Wragg, Effect of flow rate and constant operating current on the behaviour of a recirculating electrochemical reactor system, J. Appl. Electrochem. 13 (1983) 507–517.

[19] R., Lacroix, E., Roubaud, B., Erable, L., Etcheverry, A., Bergel, R., Basséguy, S., Da Silva, Design of 3D microbial anodes for microbial electrolysis cells (MEC) fuelled by domestic wastewater. Part I: Multiphysics modelling, Journal of Environmental Chemical Engineering 9 (2021).10.1016/j.jece.2021.105476.

[20] Y. Jia, M. Zeng, P. Barnoon, D. Toghraie, CFD simulation of time-dependent oxygen production in a manifold electrolyzer using a two-phase model, Int. Commun. Heat. Mass Transf. 126 (2021), 105446, https://doi.org/10.1016/j.icheatmasstransfer.2021.105446.

[21] A.S., Tijani, D., Barr, A.H., Rahim, Computational Modelling of the Flow Field of An Electrolyzer System using CFD, volume 79, Elsevier B.V., 2015.10.1016/j.egypro.2015.11.462.

[22] L. Castañeda, R. Antaño, F.F. Rivera, J.L. Nava, Computational fluid dynamic simulations of single-phase flow in a spacer-filled channel of a filter-press electrolyzer, Int. J. Electrochem. Sci. 12 (2017) 7351–7364, https://doi.org/10.20964/2017.08.09.

[23] P.C. Guo, P.C. Guo, On the influence of the nucleation overpotential on island growth in electrodeposition, Electrochimica Acta 55 (2010) 4086–4091, https://doi.org/10.1016/j.electacta.2010.02.038.

[24] A. Angulo, P. van der Linde, H. Gardeniers, M. Modestino, D. Fernández Rivas, Influence of bubbles on the energy conversion efficiency of electrochemical reactors, Joule 4 (2020) 555–579, https://doi.org/10.1016/j.joule.2020.01.005.

[25] M. Philippe, H. Jérôme, B. Sebastien, P. Gérard, Modelling and calculation of the current density distribution evolution at vertical gas-evolving electrodes, Electrochim. Acta 51 (2005) 1140–1156, https://doi.org/10.1016/j.electacta.2005.06.007.

[26] E.B. Carneiro-Neto, M.C. Lopes, E.C. Pereira, Simulation of interfacial pH changes during hydrogen evolution reaction, J. Electroanal. Chem. 765 (2016) 92–99, https://doi.org/10.1016/j.jelechem.2015.09.029.

[27] G. Wosiak, M.C. Silva, J. da Silva, E.B. Carneiro-Neto, M.C. Lopes, E. Pereira, Evaluation of interfacial pH change during water splitting at pulsed regime using finite element method, Int. J. Hydrog. Energy 46 (2021) 17644–17652, https://doi.org/10.1016/j.ijhydene.2021.02.195.

[28] G., Wosiak, J., da Silva, S.S., Sena, R.N., de Andrade, E., Pereira, Cfd simulation and experimental comparison of bubble-induced convection during electrochemical water splitting, Chemical Engineering Journal 433 (2022) 133194. ⟨https://www.sciencedirect.com/science/article/pii/S1385894721047689⟩. doi:10.1016/j.cej.2021.133194.

[29] H. Vogt, R.J. Balzer, The bubble coverage of gas-evolving electrodes in stagnant electrolytes, Electrochim. Acta 50 (2005) 2073–2079, https://doi.org/10.1016/j.electacta.2004.09.025.

[30] M. Knöppel, D. Möckl, K. Escalera-López, M. Stojanovski, T. Bierling, S. Böhm, M. Thiele, S. Rzepka, Cherevko, On the limitations in assessing stability of oxygen evolution catalysts using aqueous model electrochemical cells, Nature Communications 12 2021 10.1038/s41467–021-22296–9.

[31] A. Sokolichin, G. Eigenberger, A. Lapin, Simulation of buoyancy driven bubbly flow: established simplifications and open questions, AIChE J. 50 (2004) 24–45, https://doi.org/10.1002/aic.10003.

[32] J., Rodríguez, E., Amores, Cfd modeling and experimental validation of an alkaline water electrolysis cell for hydrogen production, Processes 8 (2020). ⟨https://www.mdpi.com/2227–9717/8/12/1634⟩.10.3390/pr8121634.

[33] K. Aldas, Application of a two-phase flow model for hydrogen evolution in an electrochemical cell, Appl. Math. Comput. 154 (2004) 507–519, https://doi.org/10.1016/S0096-3003(03)00731-8. ⟨https://www.sciencedirect.com/science/article/pii/S0096300303007318⟩.

[34] Øystein Ulleberg, Modeling of advanced alkaline electrolyzers: a system simulation approach, International Journal of Hydrogen Energy 28 (2003) 21–33.⟨https://www.sciencedirect.com/science/article/pii/S0360319902000332⟩. doi:10.1016/S0360–3199(02)00033–2.

[35] M.D., Mat, K., Aldas, O.J., Ilegbusi, A two-phase flow model for hydrogen evolution in an electrochemical cell, International Journal of Hydrogen Energy 29, 2004. 1015–1023.⟨https://www.sciencedirect.com/science/article/pii/S036031990300329X⟩. doi:10.1016/j.ijhydene.2003.11.007, fuel Cells.

[36] E. López-Fernández, C.G. Sacedón, J. Gil-Rostra, F. Yubero, A.R. González-Elipe, A. de Lucas-Consuegra, Recent advances in alkaline exchange membrane water electrolysis and electrode manufacturing, Molecules 26 (2021) 1–24, https://doi.org/10.3390/molecules26216326.

[37] R.J. Gilliam, J.W. Graydon, D.W. Kirk, S.J. Thorpe, A review of specific conductivities of potassium hydroxide solutions for various concentrations and temperatures, Int. J. Hydrog. Energy 32 (2007) 359–364, https://doi.org/10.1016/j.ijhydene.2006.10.062.
[38] K.I. Kuznetsov, S.V. Skorodumov, P.P. Granchenko, Measurements of the dynamic viscosity and density of KOH solutions at atmospheric pressure, High. Temp. 58 (2020) 806–811, https://doi.org/10.1134/S0018151×20060127.
[39] K. Zeng, D. Zhang, Recent progress in alkaline water electrolysis for hydrogen production and applications, Prog. Energy Combust. Sci. 36 (2010) 307–326, https://doi.org/10.1016/j.pecs.2009.11.002.
[40] R.V. Lenth, Quick and easy analysis of unreplicated factorials, Technometrics 31 (1989) 469–473. ⟨http://www.jstor.org/stable/1269997⟩.